



Disorders of the Nervous System

Cnih3 Deletion Dysregulates Dorsal Hippocampal Transcription across the Estrous Cycle

Bernard Mulvey,^{1,2}  Hannah E. Frye,³ Tania Lintz,³ Stuart Fass,^{1,2} Eric Tycksen,^{1,4} Elliot C. Nelson,² Jose A. Morón,³ and  Joseph D. Dougherty^{1,2}

<https://doi.org/10.1523/ENEURO.0153-22.2023>

¹Department of Genetics, Washington University School of Medicine, St. Louis, MO 63110, ²Department of Psychiatry, Washington University School of Medicine, St. Louis, MO 63110, ³Department of Anesthesiology, Washington University School of Medicine, St. Louis, MO 63110, and ⁴McDonnell Genome Institute, Washington University School of Medicine, St. Louis, MO 63110

Abstract

In females, the hippocampus, a critical brain region for coordination of learning, memory, and behavior, displays altered physiology and behavioral output across the estrous or menstrual cycle. However, the molecular effectors and cell types underlying these observed cyclic changes have only been partially characterized to date. Recently, profiling of mice null for the AMPA receptor trafficking gene *Cnih3* have demonstrated estrous-dependent phenotypes in dorsal hippocampal synaptic plasticity, composition, and learning/memory. We therefore profiled dorsal hippocampal transcriptomes from female mice in each estrous cycle stage, and contrasted it with that of males, across wild-type (WT) and *Cnih3* mutants. In wild types, we identified only subtle differences in gene expression between the sexes, while comparing estrous stages to one another revealed up to >1000 differentially expressed genes (DEGs). These estrous-responsive genes are especially enriched in gene markers of oligodendrocytes and the dentate gyrus, and in functional gene sets relating to estrogen response, potassium channels, and synaptic gene splicing. Surprisingly, *Cnih3* knock-outs (KOs) showed far broader transcriptomic differences between estrous cycle stages and males. Moreover, *Cnih3* knock-out drove subtle but extensive expression changes accentuating sex differential expression at diestrus and estrus. Altogether, our profiling highlights cell types and molecular systems potentially impacted by estrous-specific gene expression patterns in the adult dorsal hippocampus, enabling mechanistic hypothesis generation for future studies of sex-differential neuropsychiatric function and dysfunction. Moreover, these findings suggest an unrecognized role of *Cnih3* in buffering against transcriptional effects of estrus, providing a candidate molecular mechanism to explain estrus-dependent phenotypes observed with *Cnih3* loss.

Key words: candidate gene; gene expression; opioid use disorder; sex differences; sex hormones

Significance Statement

Cnih3 mutants show estrus-dependent alterations in learning, as well as physiological and anatomic changes in the dorsal hippocampus. However, the transcriptomic consequences of the estrus cycle on gene expression in the dorsal hippocampus of mice, including of *Cnih3* mutants, have not been characterized. Here, we identify candidate cell types, pathways, and gene regulators putatively involved in estrus-dependent gene expression in wild-type (WT) mice. We then contrast these with dorsal hippocampal transcriptomics in *Cnih3* knock-out (KO) mice. Using our wild-type data as a reference, we demonstrate that *Cnih3* knock-out mice have accentuated transcriptional responses across the estrus cycle.

Received April 8, 2022; accepted February 17, 2023; First published February 27, 2023.

J.D.D. has previously received royalties for Translating Ribosome Affinity Purification, a methodology not utilized in this manuscript. All other authors declare no competing financial interests.

Author contributions: H.E.F., T.L., E.C.N., J.A.M., and J.D.D. designed research; H.E.F. and T.L. performed research; B.M., S.F., and E.T. analyzed data; B.M., T.L., S.F., E.C.N., J.A.M., and J.D.D. wrote the paper.

Introduction

Neurobehavioral sex differences are well-established factors in physiologic and pathologic processes ranging from reproduction and parenting to depression and addiction, in part through acute “activational” effects of sex hormones (Arnold, 2009). Example activational effects include regulation of dopamine turnover, suppression of GABA signaling (Del Río et al., 2018), and estrogenic stimulation of corticosteroid release through hypothalamic-pituitary-adrenal (HPA) axis upregulation of *CRH* (in contrast to its repression by androgens; Lund et al., 2004; Bao et al., 2006). Perhaps unsurprisingly, then, the human menstrual and rodent estrous cycles continually alter the microstructure of the brain: sex-specific responses to social stress in rat medial prefrontal cortex have implicated estrous-dependent alterations to cellular communication (Duclot and Kabbaj, 2015).

Phenotypically, the impact of sex has been observed in neuropsychiatric diseases and rodent models thereof (Kuhn, 2015), partly by way of the hippocampus in addiction (Kohtz and Aston-Jones, 2016). Hippocampal synaptic density peaks during proestrus, when estradiol and progesterone are highest (Woolley and McEwen, 1992), affecting learning and memory (Frick et al., 2015; Frick and Kim, 2018). In the mouse hippocampus, this increase in synaptic density is accompanied by elevated expression of synaptic transmission genes during proestrus and diestrus in comparison to males (Jaric et al., 2019). A longitudinal human study across the menstrual cycle revealed hippocampal changes suggestive of increased myelination during high estrogen periods (Barth et al., 2016), paralleling changes seen in rodent models during short-term learning. Despite such physiologic and behavioral observations, however, characterization of their potential molecular mediators has been less intensive to date.

The dorsal hippocampus, an interface of stress, sex, and drug-seeking behavior (Henderson et al., 2015; Johnson et al., 2021), is essential for drug-induced associative learning (Fakira et al., 2016). Consistent with this, mouse knock-out (KO) of the opioid dependence-associated gene *Cnih3* (Nelson et al., 2016) results in not only sex- but estrous-stage-specific effects on learning and memory (H.E. Frye et al., 2021). *Cnih3* is an AMPA receptor (AMPA) trafficking protein that delivers AMPARs to the postsynaptic membrane, enhancing their activity (Schwenk et al., 2009; Coombs et al., 2012; Herring et al., 2013; Shanks et al., 2014; Brown et al., 2018). Hippocampal AMPARs have a clear role in learning and memory (Lee et al., 2003; Kessels

and Malinow, 2009); accordingly, *Cnih3* KO showed severe memory deficits, altered biochemical localization of AMPARs, and corresponding synaptic changes, *but* only in female mice, and limited to particular phases of the estrous cycle (H.E. Frye et al., 2021). This suggested the surprising hypothesis that *Cnih3* is involved in buffering the female brain against cyclic changes in hippocampal learning.

A recent synthesis across several studies of wild-type (WT) mouse hippocampus found that very few genes are consistently called sex DE (Ocañas et al., 2022). The granular manner in which the estrous cycle alters brain gene expression and pathways, even in WT rodents, has only been characterized in limited phases (Iqbal et al., 2020) or not yet in direct contrast to males (DiCarlo et al., 2017). Therefore, we first sought to determine how extensively WT dorsal hippocampal gene expression fluctuates across estrous, as grouping all females together may underlie the reported paucity of sex DEGs via unaccounted-for biological variance and/or net male-equivocal expression. Given recent evidence of dorsal hippocampal *Cnih3* expression and cycle-dependent cellular and plasticity changes with *Cnih3* loss (H.E. Frye et al., 2021), we then sought to transcriptionally characterize the mouse dorsal hippocampus at each stage of the estrous cycle in *Cnih3* KO mice to clarify the molecular effects of KO.

In WTs, we only identify male-female divergence of autosomal gene expression when considering individual estrous stages. Using gene pattern analysis, we define cyclic expression patterns of the female dorsal hippocampus and these patterns' enrichment in cell type markers, related transcriptomic signatures, and candidate regulators, providing an extensive resource for hypothesis generation in the study of interplay between estrous and dorsal hippocampal function. We then examined differences between *Cnih3* KO males and KO females in specific phases of estrous and identified a profound enhancement in gene expression differences, resulting in substantially more differential genes between sexes.

Finally, we examined expression differences between WT versus KO altogether, in males and in each estrous stage. These analyses, when compared with those within KOs or WTs, suggested that subtle changes were being induced by *Cnih3* KO to accentuate sex-differential expression. Indeed, we observed that the magnitude of sex-differential expression at diestrus or estrus was greater in the KO regardless of false discovery rate (FDR) level, supporting the hypothesis that *Cnih3* buffers against excess gene-regulatory responses to cycling sex hormones.

Materials and Methods

Animals, estrous staging, and dorsal hippocampal dissections

Procedures were approved by the Institutional Animal Care and Use Committee at Washington University in St. Louis. Adult (age range 12–24 weeks; see Extended Data Table 1-1) WT and *Cnih3* KO littermates on a C57/BL6j background (>10 backcrossed generations) were used. This *Cnih3* KO mouse line was previously generated

This work was supported by National Institutes of Health Grants R33DA041883 and R01DA042499 and the Simons Foundation Grant 734069.

Acknowledgments: We thank Lexi Harris, Kristy Bergmann, and Jessica Higginbotham for their assistance. Figure 1 was created using BioRender.

Correspondence should be addressed to Joseph D. Dougherty at jdougherty@wustl.edu.

<https://doi.org/10.1523/ENEURO.0153-22.2023>

Copyright © 2023 Mulvey et al.

This is an open-access article distributed under the terms of the Creative Commons Attribution 4.0 International license, which permits unrestricted use, distribution and reproduction in any medium provided that the original work is properly attributed.

beginning in 2015 from *Cnih3*^{tm1a(KOMP)Wtsi} BL/6N mice (Knockout Mouse Project); full details of the KO line were previously published (H.E. Frye et al., 2021). Briefly, the KO line lacks exon four of *Cnih3*, frameshifting exons 5 and 6 and thus truncating the CNIH3 protein. We confirmed the previously reported loss of exon 4 in our experimental animals by examining alignment of RNA-sequencing (RNA-seq) reads within the *Cnih3* transcript (Extended Data Figs. 4-1, 4-2). Genotyping was performed according to methods used by the group publishing the mouse line (H.E. Frye et al., 2021). *Cnih3* heterozygotes were mated in pairs (or occasionally to *Cnih3* homozygotes) to generate homozygous KO offspring for RNA-seq. Because of the large number of mice required to cover all estrous cycle stages in two genotypes in the midst of pandemic-era animal facility constraints, mice we subsequently refer to as WT were collected from a mix of offspring from WT B6 x WT B6 matings and *Cnih3* mutant-negative littermates from *Cnih3* heterozygote x *Cnih3* heterozygote matings (parental genotypes given in Extended Data Table 1-1). Principal component analysis (PCA; Extended Data Fig. 1-2) did not identify a clear axis of variation relating to parental genotype in the WT animals; thus, we collapsed all wild-type animals together in a single group, regardless of parent genotype.

Mice were kept in climate-controlled facilities with a 12/12 h light/dark cycle and *ad libitum* access to food and water. The estrous cycle was monitored by vaginal lavage of sterile saline for at least two consecutive days before tissue harvesting. Samples were allowed to dry on glass slides, rinsed with water, and stained with giemsa stain (Ricca Chemical) to improve contrast and differentiate between cell types. Vaginal cell cytological analysis was used to identify estrous cycle stages by three independent observers. Estrus (E, Est) was characterized by the presence of cornified epithelial cells, metestrus (M, Met) by a mix of leukocytes and both nucleated and cornified epithelial cells, diestrus (D, Di) by leukocytes, and proestrus (P, Pro) by nucleated epithelial cells. Males and females at each stage of the estrous cycle ($n = 4-7$ per group) were decapitated and dorsal hippocampi were rapidly dissected over ice by a single researcher in the afternoon using methods previously described (Xia et al., 2011; Portugal et al., 2014; Fakira et al., 2016), and tissue was snap frozen on dry ice and stored at -80°C until use. Besides estrous staging before decapitation, mice used in this study were not used for anything other than the RNAseq analysis. In order to ensure responsible and judicious use of animal specimens, additional brain regions and samples were banked for potential future use in other studies.

Tissue processing and RNA purification

The dorsal-most 1/3 of each hippocampus was collected for RNA preparation. Hippocampi were placed in 500 μl of buffer [50 mM Tris, pH 7.4, 100 mM NaCl, 1% NP-40, supplemented with Rnasin (Promega) and protease inhibitors (Roche)] on ice. Samples were homogenized in buffer solution on ice using a handheld motorized pellet pestle, and lysate was then centrifuged at $2000 \times g$ for 15 min at 4°C , and 133 μl of the supernatant was taken for

RNA purification. This was mixed with 67 μl of Promega's simplyRNA Tissue kit Homogenization buffer with 1-thioglycerol (20 $\mu\text{l}/\text{ml}$), then 200 μl of the Promega kit's lysis buffer, and extracted using a Maxwell RSC 48 robot (Promega) following the manufacturer's instructions.

RNAseq library preparation and sequencing

Total RNA integrity was determined using Agilent Bioanalyzer or 4200 TapeStation. Library preparation was performed with 10 ng of total RNA for samples with a Bioanalyzer RIN score >8.0 . The resulting Poly-A enriched, double-stranded cDNA (dscDNA) was prepared using the SMARTer Ultra Low RNA kit for Illumina Sequencing (Takara-Clontech) per manufacturer's protocol. cDNA was fragmented using a Covaris E220 sonicator using peak incident power 18, duty factor 20%, cycles per burst 50 for 120 s. cDNA was blunt ended, had an A base added to the 3' ends, and then had Illumina sequencing adapters ligated to the ends. Ligated fragments were then amplified for 14 cycles using primers incorporating unique dual index tags according to manufacturer's protocol. Fragments were sequenced on an Illumina NovaSeq-6000 using paired end reads extending 150 bases.

Quantitative PCR and analysis

Using the same RNA as collected above, we synthesized single-stranded cDNA from 125 ng of each sample RNA using the qScript Reverse Transcriptase kit (QuantaBio #95047) per manufacturer instructions in 20- μl reactions. Six of these RNA samples were also prepared in a second reaction with 125 ng input RNA but no reverse transcriptase enzyme as a negative control for the quantitative PCR (qPCR) reactions. A total of 200- μl water was added to each reaction after completion, and 4 μl of the diluted reaction used as template for each qPCR reaction well. A total of 384-well plates were prepared with technical triplicate reactions (i.e., three reactions with 4 μl cDNA each) per sample for each of two genes: one gene of interest, and β -actin as within-sample normalization controls; 6 μl of a mastermix comprised of 5 μl per reaction of PowerUp SyBr Green 2 \times Mastermix (Applied Biosciences #A25742) and 0.5 μl per reaction of each primer at 10 μM (final concentration 500 nM) was added to each well of cDNA for a total of 10 μl . The primers used were: β -actin forward, 5'-AGAGGGAAATCGTGC GTGAC-3'; β -actin reverse, 5'-CAATAGTGATGACCTGG CCGT-3'; *Otx2* forward, 5'-GAATCCAGGGTGCAGGTAT GG-3'; *Otx2* reverse, 5'-CTGAAC TCACTTCCCGAGCTG-3'; *Prlr* forward, 5'-CTGCACTTGCTTACATGCTGC-3'; *Prlr* reverse, 5'-GGGGAACGACATTTGTGGATTTC-3'; *Prl* forward, 5'-CCAATCTGTTCCGCTGGTGA-3'; and *Prl* reverse, 5'-GGGACTTTCAGGGCTTGTTC-3'. A 3 min 95°C hot-start step was followed by 40 cycles of 95°C for 15 s and 63°C (annealing + elongation) for 20 s. Immediately after, a 95°C hold for 15 s and a temperature ramp from 60°C to 95°C were executed for melt curve analysis. Cycling, threshold detection, and melt curve analysis for each plate was performed on a Quantstudio 6 instrument. Wells without amplification, with melt curve peaks under 80°C , or

diverging ≥ 1 cycle to threshold of detection (CT) from the other two technical replicates for a sample were discarded from analysis if the other two wells strongly reflected one another. Delta CT (dCT) between the target gene and actin was calculated for each technical replicate of the target gene within a sample by subtracting that sample's mean actin CT. These repeated measurements were used as input for plotting as box-plots in Extended Data Figure 2-4 and used in a repeated-measures ANOVA to test each pairwise comparison of interest as defined by the RNA-seq data. Twelve total comparisons of interest were investigated across the three target genes. In all cases, no-reverse-transcriptase negative controls produced either no products, only primer dimers, or the target product but at >5 CT later than any reverse transcribed sample on the plate.

Data analysis

RNA-seq reads were aligned to the Ensembl release 101 primary assembly (GRCm38.101) with STAR version 2.7.9a (Dobin et al., 2013). Gene counts were derived from the number of uniquely aligned unambiguous reads by Subread:featureCount version 2.0.3. All gene counts were then imported into the R/Bioconductor package EdgeR (Robinson et al., 2010) and TMM normalization size factors were calculated to adjust for samples for differences in library size. Ribosomal genes and genes not expressed in at least ten samples greater than one count-per-million were excluded from further analysis. The TMM size factors and the matrix of counts were then imported into the R/Bioconductor package Limma (Ritchie et al., 2015). Weighted likelihoods based on the observed mean-variance relationship of every gene and sample (i.e., one model for all 10 groups, each estrous stage/males and each genotype) were then calculated for all samples and the count matrix was transformed to moderated log₂ counts-per-million with Limma's voomWithQualityWeights (Liu et al., 2015). Differential expression analysis was then performed to analyze for differences between pairs of conditions; results were filtered to genes with Benjamini-Hochberg FDR adjusted *p*-values less than or equal to 0.05 except where noted. All differential expression analyses used a single input dataset covering all WT and *Cnih3* KO samples and model using a Limma contrast matrix to avoid the need for *post hoc* multiple testing corrections: $expression \sim 0 + group$ (where group = genotype and estrous stage or male). Estrous-stage agnostic and sex-agnostic (global genotype effect) contrasts were collapsed into aggregated contrast coefficients for each stage together; for example, *WT female versus WT male DE = (0.25*metestrus + 0.25*diestrus ...) - male*.

Using the ssizeRNA package in R, we estimated that our experiment as executed was powered with $\beta = 0.862$ for an FDR threshold of 0.05 with a sample size of 6 per group, 5% of genes as DE at $|FC|$ of $\geq \pm 2$, mean count of 3000 (based on the analyzed counts table), and the global dispersion, which by nature will be influenced by age variability across the cohort, of the analyzed counts (0.048).

Because of the number of mice and conditions to be collected, ages were not ideally balanced in the dataset. As brain gene expression differences in B6 lineage mice

from ages one to four months have been observed (Bundy et al., 2017), we investigated whether age had a substantial impact on our results. We used the R package ComBat-seq (Zhang et al., 2020) to remove age effects (with age as categorical effect in months) while preserving genotype-stage/sex effects before a parallel, exploratory limma analysis. This two-step procedure constituted first correcting the library-size-corrected counts for age using ComBat-seq, followed by the same limma-voom steps as used in the original analysis (see below, Code availability). 3D principal component analysis (PCA) was used to compare the age-adjusted data to the original analysis (Extended Data Fig. 1-1).

For gene pattern analysis, the degPatterns function of R package DEGreports package (Pantano et al., 2022) was used with the moderated log₂ counts per million (CPM) expression values for an input gene set to examine the patterns of expression over each stage/condition examined. The degPatterns parameters used were as follows: minimum number of genes fitting a pattern to report the pattern is 5 (*minc* = 5) and outliers were excluded from final clusters (*reduce* = TRUE).

For ontology, cell type, and regulatory enrichments, the Enrichr web tool (E.Y. Chen et al., 2013) was used, entering the list of significant differentially expressed genes (DEGs; at FDR < 0.05) from the differential expression analysis directly or those DEGs derived from the clustering analyses previously described. Result tables were downloaded from each Enrichr query database of interest if that result table contained at least one putatively brain-relevant, *q*-value significant enrichment being driven by at least five of the input genes (or, in cases of large gene sets, at least eight; specified in corresponding figure legends). Result tables were then collated across databases in R (see below, Code availability).

Comparison to DEGs from prior studies

WT stage-stage comparisons for dorsal hippocampus were compared to significant DEGs previously reported between estrous stages in Table 4 of DiCarlo et al, 2017. Each direction of effect was separated into its own column (two directions by six comparisons = 12 columns). Genes listed in DiCarlo that did not meet filtering criteria for analysis in our study were removed. For the genes analyzed in both our study and in DiCarlo et al., 2017; we programmatically obtained the number of previously reported DEGs with concordant effect directions (e.g., proestrus $>$ diestrus) in our data both without statistical thresholds and at an FDR threshold of 0.05 (see below, Code availability).

Data availability

Data are available at GEO under accession GSE199722. Reviewer token, if needed, is zzybsiectzotpwrt.

Code availability

Code for read QC, alignment, and filtering is available from the authors on request. The raw unfiltered counts, a filtered count matrix as used for analysis, code to analyze

the filtered counts in limma, and scripts for all analyses/plotting thereafter (with the exception of Enrichr analyses themselves, which were executed and collected through the Enrichr web tool) are available on Bitbucket at <https://bitbucket.org/jdlabteam/workspace/projects/CHER>.

Results

Wild-type dorsal hippocampal gene expression: sex and estrous differences

Gene expression between wild-type male and female bulk dorsal hippocampus does not substantially differ

As collection of this cohort of mice required some flexibility in terms of mouse age (given size and number of conditions), we first examined whether age played a substantial, statistically-adjustable role in our differential expression analyses. Using the ComBat-seq package in R, we specified the same model (see Materials and Methods) with an additional covariate of age (categorically, in months) as a potential confounding variable to be adjusted for. We compared three-dimensional PCA plots of the limma model fits with and without preceding ComBat-seq correction to determine whether age correction altered the relationships among RNA-seq samples. These plots visually suggested (Extended Data Fig. 1-1) a modest relationship between principal component 2 (PC2) and age. However, PC2 explained 12.1% of variance in the original data, while still explaining 10.3% of variance in the age-negated data, confirming that age did not substantially influence our results (i.e., only ~2% of the cohort-wide variance was attributable to age). We therefore did not adjust for age in the analyses that follow.

We first tested the 16,168 genes in our wild-type (WT) dorsal hippocampal RNA-seq data for female gene expression differences from male, examining both estrous-naive and stage-specific differences in gene expression (Figs. 1B, 2; Extended Data Table 2-1A). At the level of sex alone, we only detected six differentially expressed genes (DEGs; FDR < 0.05, no log fold-change threshold), all from the sex chromosomes (Fig. 2A). Examining nominally significant DEGs with a log fold-change (FC) exceeding 1.5 revealed four additional genes, including *Depp1* (female-upregulated, logFC 2.3, $p < 4 \times 10^{-3}$) and *Avpr1b* (female-upregulated, logFC 2.13, $p < 2 \times 10^{-3}$). In all, the “net” female dorsal hippocampal transcriptome did not diverge appreciably from male.

As prior experiments with *Cnih3* have illustrated, male-female differences can be influenced by the stage of the estrous cycle (H.E. Frye et al., 2021). Therefore, we performed comparisons between WT male and WT females for each estrous stage separately, identifying 65 unique genes as significant across the four comparisons (Fig. 2B, C; Extended Data Table 2-1B,E). For metestrus (Met) and proestrus (Pro), and most surprisingly, estrus (Est), we only identified sex chromosomal genes as DEGs (FDR < 0.05) when compared with male. In contrast, we identified 62 significant DEGs in diestrus (Di) compared with male, 57 of which were unique to this stage (eight female-upregulated, 49 male-upregulated; these did not include *Cnih3*, consistent with qPCR reports; H.E. Frye et al., 2021).

Altogether, these findings suggest that the female dorsal hippocampus only diverges to any appreciable extent from males during diestrus.

Gene expression changes substantially across estrous stages within WT females

We next examined the female samples alone, comparing each estrous stage to each other stage to identify genes significantly fluctuating over the course of the estrous cycle. Strikingly, we identified over 5000 unique DEGs (FDR < 0.05, no logFC threshold) between at least one pair of stages of the 6 combinations possible (Fig. 2D,E; Extended Data Table 2-1F-K). There were no significant DEGs between Met and Est, while the other 5 pairwise comparisons yielded 105–4004 significant DEGs each. Quantitative PCR (qPCR) performed using the RNA from this entire cohort of animals verified large-magnitude changes observed in the sequencing, confirming the accuracy of our sequencing and analysis (Extended Data Fig. 2-4).

Altogether, these findings suggest that male dorsal hippocampal gene expression diverges neither from females overall, nor appreciably from individual estrous stages. Instead, most variability in expression is constrained to females in an estrous stage-dependent manner. Diestrus appears to correspond to the most distinctive transcriptional state of the dorsal hippocampus in that it is the most distinct from both males and other estrous stages (in terms of DEG) at respectively modest and sprawling scales.

We noted a striking increase in number of DEGs between pairs of estrous stages observed here compared with prior work. To ensure our analysis was consistent with prior studies of estrous effects on WT hippocampal gene expression, we compared our results to available published data. A prior study of WT rat dorsal and ventral hippocampus identified 37 DEGs between proestrus and estrus, validating seven of them by qPCR (Iqbal et al., 2020). Despite species and region/subregion differences between this study and ours, we observed significant DE for three of those seven genes between proestrus and estrus. We confirmed overall patterns of estrous DE by comparing our directions of effect with those of significant DEGs from a prior study of mouse hippocampus (DiCarlo et al., 2017). We noticed relatively limited FDR < 0.05 replication between the current data and that from DiCarlo. We interpreted comparisons in terms of DE significance cautiously, as we could not determine whether the DEGs reported in that study were called with a fold-change minimum, and as the prior study's results were generated using the DESeq package, which has been shown to be prone to false positives in large/multivariate sequencing analyses (Li et al., 2022), and does not account for genewise variance patterns, in contrast to the limma-voom analysis employed here (Liu et al., 2015). However, when solely comparing directional relationships without statistical thresholds imposed on our data for the two largest gene sets from their data (proestrus > estrus; diestrus < proestrus), 100% of our effect directions were in agreement (Extended Data Fig. 2-1). We therefore attribute the sharp increase in estrous-regulated genes detected here to our analysis strategy's

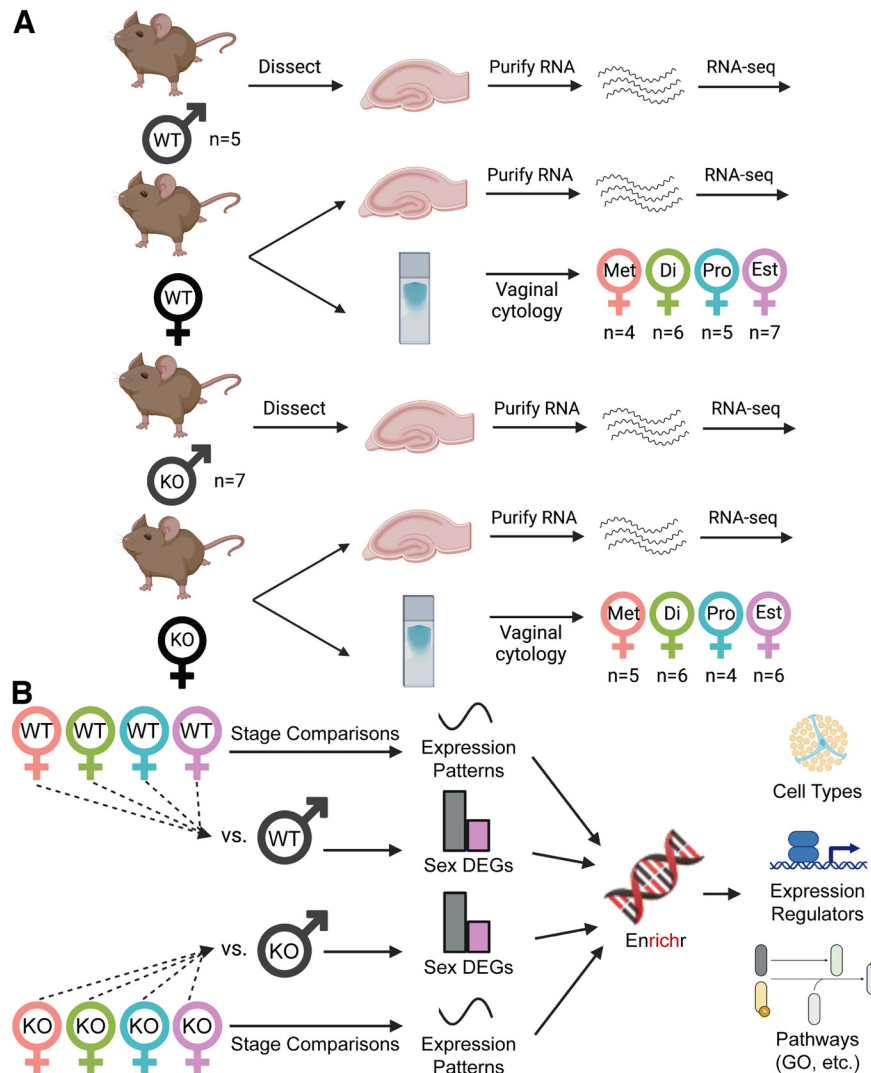


Figure 1. Experimental workflow. **A**, Dorsal hippocampi from male and female adult C57/B6 wild-type (WT) and *Cnih3* knock-out (KO) mice were collected for RNA-seq (one hippocampus/mouse = one sample). Vaginal cytology was performed at time of tissue collection. Estrous stage was independently determined from cytology by two to three scorers. Final *n* for each genotype and estrous stage group are indicated in the figure. **B**, Analytic workflow. Sequencing QC results and mouse metadata are included in Extended Data Table 1-1. Additional QC in the form of principal component analyses with and without adjustment for mouse age are in Extended Data Figure 1-1. Met = metestrus; Di = diestrus; Pro = proestrus; Est = estrus.

variance control, sample size, and potentially to differences in use of fold-change thresholds.

Gene expression patterns in WT dorsal hippocampus across the estrous cycle

Given the large number of pairwise DEGs identified between different stages of the estrous cycle, we were well-powered to cluster these genes by their rise and fall across the cycle to predict putative biological functions subject to estrous influence in the dorsal hippocampus. Characterization of these patterns resulted in a resource for hypothesis generation concerning sex differences in the dorsal hippocampus, including as a comparator for subsequent expression profiling of *Cnih3* KO. In addition to the provided results from stage-stage comparisons (Extended Data Table 2-1F–

K), we present a series of gestalt analyses to understand these differences below.

To clump genes by their cyclic pattern of expression, we used the *DEGReport* package's *degPatterns* function in R 4.1.2, and clustered the union of genes significant at an FDR < 0.01 (1700 genes total) from any estrous comparison above. We identified five gene expression patterns total in WT (Fig. 3A; Extended Data Table 3-1A), the majority of which fell into clusters corresponding to peak expression in diestrus (cluster 4), trough expression at diestrus (clusters 1 and 2), or peak expression at proestrus (clusters 1 and 3). We next analyzed each cluster's genes for specific biological pathways using the *Enrichr* tool (E.Y. Chen et al., 2013). *Enrichr* annotations of note for four of these clusters (1–4) highlighted several pertinent aspects of brain and hormonal biology (Extended Data

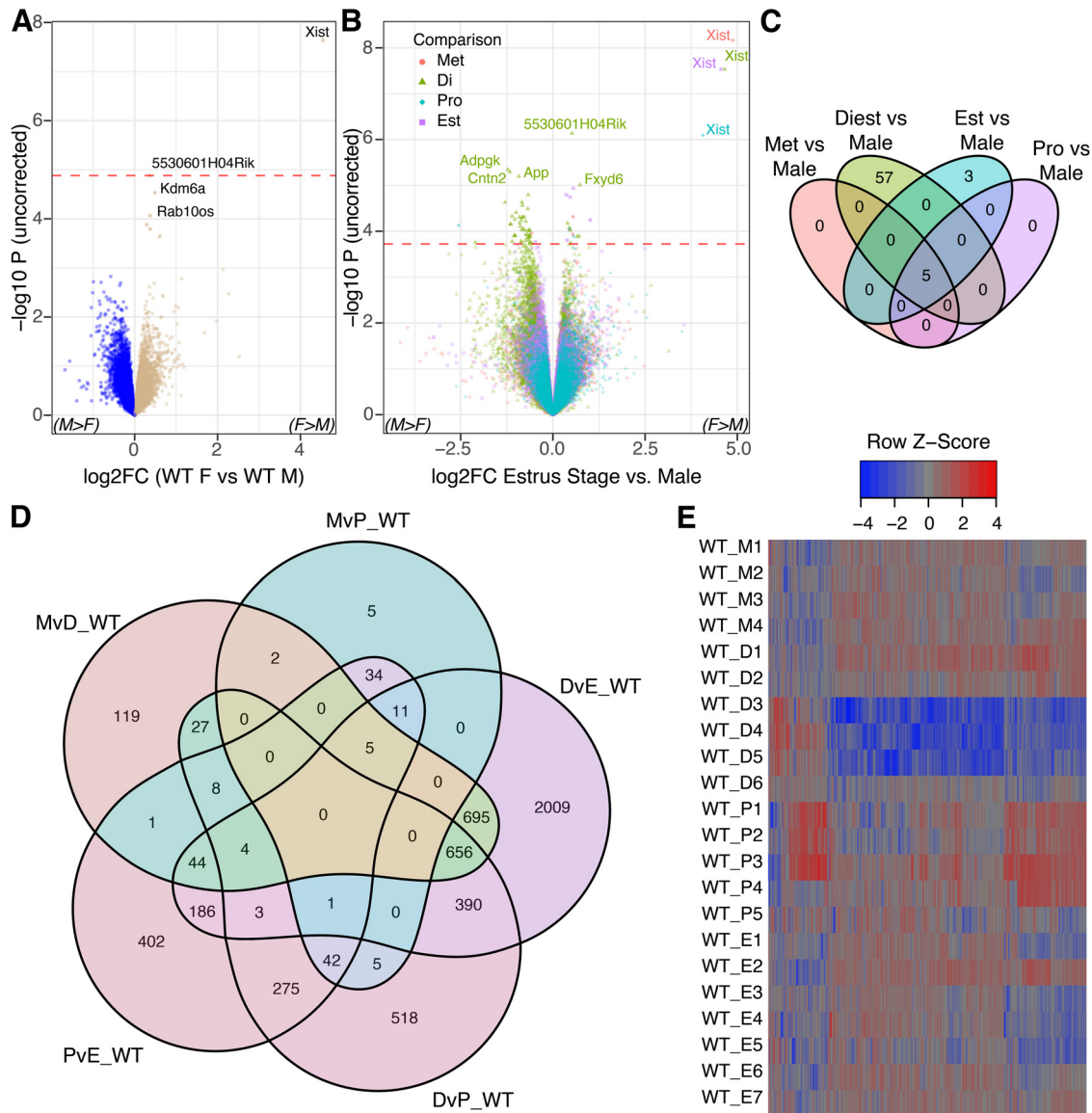


Figure 2. Wild-type dorsal hippocampal transcriptome varies across estrous stages. **A**, Volcano plot illustrating the effective absence of sex-differential genes when comparing wild-type males to females combined across all stages of the estrous cycle. Female enriched genes are positive. **B**, A joint volcano of differential expression analysis results for each estrous stage compared with males. The largest magnitude differences in gene expression are between diestrus and males. *Xist* is shown on the plot to illustrate the comparative magnitude of sex-specific gene expression from the sex chromosomes; Y-chromosome genes are excluded for scale. **C**, Venn diagram illustrating the number of significant DEGs between males and females for each estrous stage. The majority of differential expression occurs in diestrus (see also replication of stagewise differential expression compared with a prior study of hippocampus in Extended Data Fig. 2-1). **D**, A Venn diagram of differentially expressed genes across pairwise comparisons of estrous stages, illustrating the dependence of the female hippocampal transcriptome on estrous stage. Once again, diestrus is the most distinctive of the four stages. Full RNA-seq analysis results for comparisons in panels **A–D** are included in Extended Data Table 2-1. **E**, Heatmap of samplewise expression of the same genes as in panel **D**. Hippocampal gene expression changes across estrous stages are individually subtle but extensive in terms of the number of genes involved. Additional clustering of gene expression by genotype and sex/estrous stage is in Extended Data Figures 2-2 and 2-3. Pairwise comparisons at or near statistical significance for three genes were directionally verified and significant by qPCR using the same RNA as sequenced (Extended Data Fig. 2-4).

Table 3-1B). WT estrous cluster 1, characterized by peak expression in proestrus and trough expression in diestrus (Fig. 3A), was enriched for oligodendrocyte marker genes (Fig. 3B). (Indeed, 4/6 of the stagewise comparisons above showed differential expression of *Gal3st1*,

whose protein product sulfonates carbohydrates in sphingolipids to produce sulfatide, a major component of myelin). Cluster 2, also characterized by trough expression in diestrus but with estrus-metestrus peak expression, showed enrichment for genes in “early estrogen response,” calcium

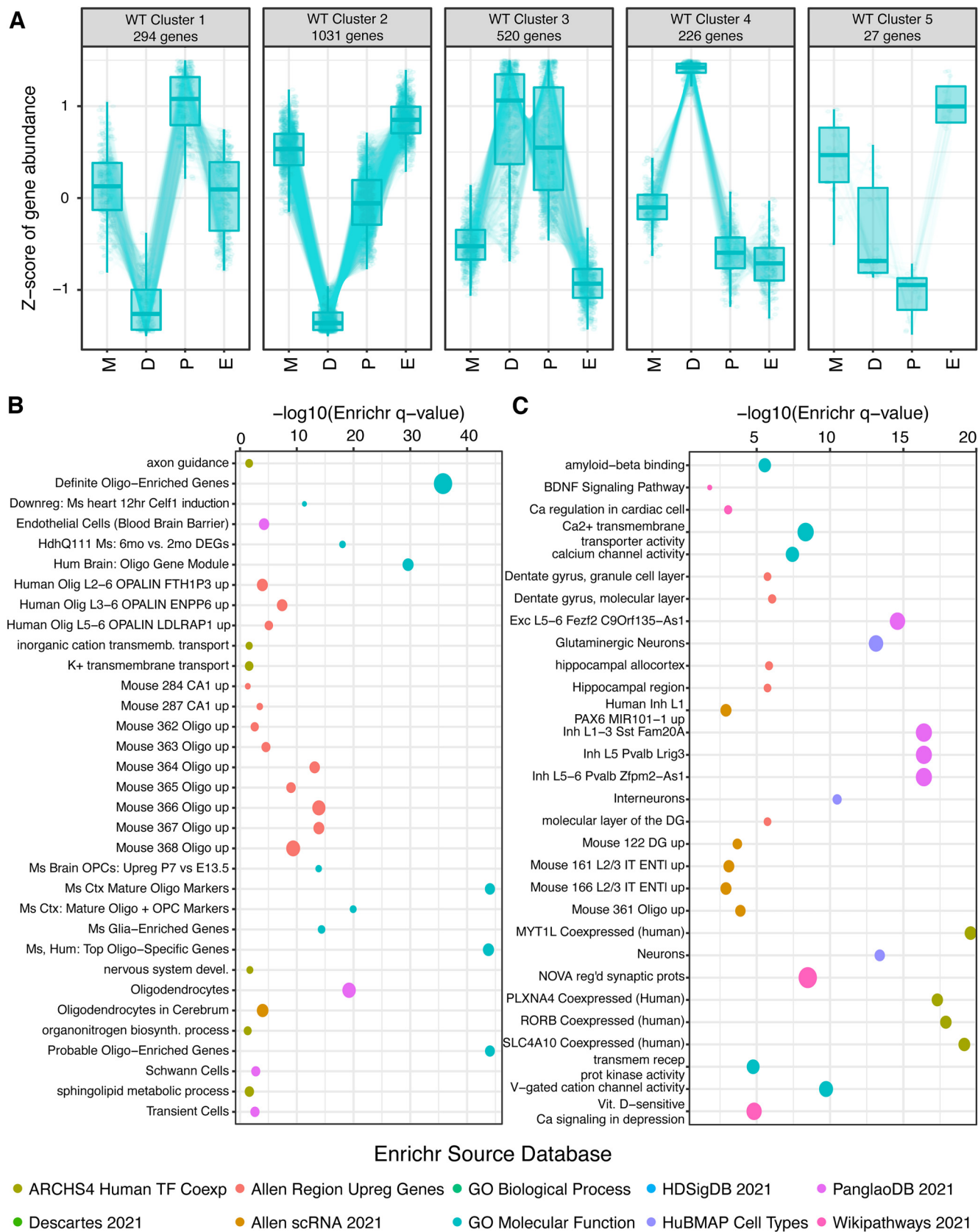


Figure 3. Wild-type female cyclic hippocampal gene expression patterns across estrous. **A**, Patterning analysis of gene expression for DEGs between any pair of stages at FDR < 0.01 identifies five clusters of expression fluctuation across the estrous cycle. **B**, Selected Enrichr analysis results for cluster 1 from panel **A**. Specific terms are highlighted in the plot, all with log odds ratio (OR) of

continued

the cluster gene set >2.5 , all enrichment (uncorrected) p -values < 0.05 , with more than or equal to eight genes from the cluster included in the enriched annotation term. Point colors indicate which Enrichr dataset each term comes from, while point sizes are scaled to the log OR. **C**, Selected Enrichr analysis results for cluster 2 from panel **A**. All terms meet the same filtering criteria as in panel **B**. Gene-to-cluster assignments and complete Enrichr results are given in Extended Data Table 3-1.

signaling, glutamate receptor signaling, and axon guidance, as well as strong enrichment for inhibitory interneuron subtypes, glycinergic neurons, and all classes of glia, and finally regional enrichment for the molecular layer of the dentate gyrus (Fig. 3A,C). By contrast, WT estrous cluster 3, with peak expression across diestrus and proestrus, was enriched for protein interactors of estrogen receptor *Esr1* with only weak enrichment for dopaminergic, glycinergic, and subtype-nonspecific neuron markers (Extended Data Table 3-1B). Finally, cluster 4, representing genes sharply peaking in diestrus, was strongly enriched for *Sncg*⁺ neurons and hippocampal CA3 neurons from Allen Brain Atlas single-cell RNA-seq. Cluster four was also enriched for genes upregulated by knock-down of *RELA*, *Neurod1*, or *Mecp2*, or by overexpression of *Neurog3* (Extended Data Table 3-1B). As some of these TFs are known regulators of neuronal gene expression, this suggests neuronal gene expression is disproportionately altered in this cyclic manner. Reassuringly, the pathway analyses highlight CNS pathways and cell types, rather than those of other tissues, consistent with a bona fide estrous cycle impact on the brain. These findings highlight higher-order biological changes in the dorsal hippocampus occurring at different stages in the estrous cycle.

Cnih3 knock-out effects on dorsal hippocampus

We first examined KO and WT *Cnih3* sequencing alignments to confirm that *Cnih3* exon four was indeed absent, as expected for this mouse line (Extended Data Figs. 4-1, 4-2). This mutation induces a frameshift and thus predicted loss of function in *Cnih3*. Subsequently, we examined expression of all genes for the KO mice in the same series of approaches as for WT above, which are on the whole presented in a similar structure to those above for sake of comparability. We then performed KO versus WT comparisons for each sex/estrous stage, and finally, we describe the overall key patterns of transcriptomic alterations identified in the *Cnih3* KO dorsal hippocampus.

Gene expression differences between Cnih3 KO males and females are subtle but far outnumber WT sex differences

Cnih3 KO males ($n = 7$) and females (all estrous stages considered jointly, $n = 21$) showed much starker differential expression in the dorsal hippocampus, with 849 genes detected as differentially expressed at $FDR < 0.05$ (Fig. 4A; Extended Data Table 4-1A). Notably, only 18.6% of these genes had an absolute logFC exceeding 0.5, suggesting the vast majority of estrous-nonspecific, sex-differential expression in the *Cnih3* KO dorsal hippocampus remains subtle in nature. By contrast, two autosomal genes showed large, FDR-significant sex effects with a logFC of > 1.5 : perilipin 4 (*Plin4*) and prolactin (*Prl*), the latter having only achieved nominal significance in WT male-female DE analysis.

Quantitative PCR (qPCR) performed using the RNA from this entire cohort of animals confirmed large-magnitude differential expression between several pairs of stages and between the sexes in KO mice, including for *Prl* (Extended Data Fig. 2-4).

Considering the estrous stage-specific sex differences in behavior and dorsal hippocampal architecture previously described in *Cnih3* KO mice (H.E. Frye et al., 2021), we also examined males compared with each stage of the estrous cycle independently (Fig. 4B; Extended Data Table 4-1B-E). Here, we also detected a far greater number of DEGs compared with the same approach in WT: an 80-fold greater number of unique DEGs across the four KO comparisons, totaling 5245, compared with the 65 from the four contrasts in WT. The overall distribution of DE events was similar to WT, albeit on a much larger scale, with 54, 4510, 36, and 1146 DEGs for Met, Di, Pro, and Est, respectively, compared with males (Fig. 4C,D). Likewise, the number of high-magnitude ($\log FC > 1.5$) DE events for Di versus males totaled 145 in KO, versus six in WT. Altogether, these findings suggest that *Cnih3* knock-out accentuates sex-differential gene expression in both a global and estrous stage-specific manner.

Cnih3 KO females retain WT estrous expression patterns outside of small sets of proestrus-stimulated genes

As in our WT data, we then performed pairwise comparisons of estrous stages in the *Cnih3* KO samples (Extended Data Table 4-1F-K). On the whole, these differential expression sets were comparable in size, with the exception of substantial increases in the number of FDR significant DEGs between Di-Pro and Di-Est for KO relative to WT (increases of ~ 3400 and ~ 800 genes, respectively; Fig. 4E). Despite the similar gene set sizes, the DEGs between the WT and KO comparisons were only ~ 40 – 50% shared (Fig. 4E), additionally suggesting perturbations to ordinary estrous cycle gene expression.

To clarify whether the broad-scale cyclic patterns of gene expression across the estrous cycle we identified in WT above were intact in *Cnih3* KO mice, we Z-scored the KO expression levels of the same genes and overlaid them into the WT clustering space to compare their cyclic expression to WT (Fig. 5A). While many clustering patterns seemed to be generally retained, if sometimes with larger gene-set level variance in KO, there were notable discrepancies between WT and KO cycling patterns for clusters 1 and 3, two clusters defined by genes with peak expression in proestrus.

To further dissect the alterations to clusters 1 and 3, we re-performed clustering on the genes defining the WT cluster using KO and WT data combined, resulting in 4 and 7 subclusters of expression, respectively (i.e., subclusters with a specific pattern in WT and a specific pattern in KO; we call these, e.g., cluster 3.1, 3.2...). This co-visualization,

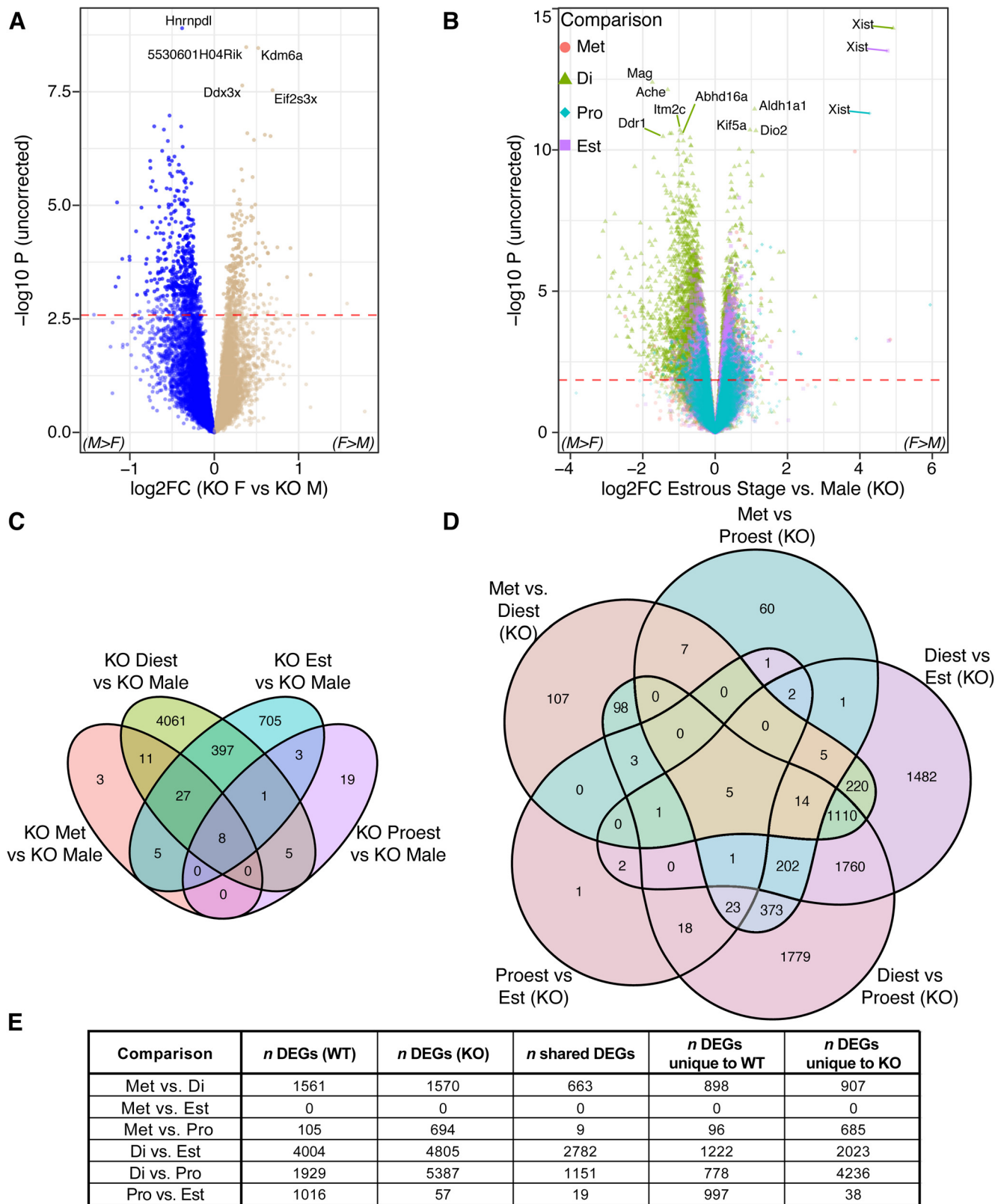


Figure 4. *Cnih3* knock-out hippocampal transcriptome shows greater differences between sexes and estrous stages. The knock-out effect on *Cnih3* exons shown in Extended Data Figures 4-1 and 4-2 confirmed the KO genotype for all assessed mice. **A**, At the level of males compared with all females, the *Cnih3* knock-out line shows a substantial increase in the number of significant DEGs compared with WT (Fig. 2A). **B**, A joint volcano of differential expression analysis results for each KO estrous stage compared with KO males. The largest magnitude differences in gene expression are between diestrus and males, consistent with the WT pattern of

continued

diestrus constituting the most distinct transcriptional state. **C**, Likewise, the greatest number of DEGs between males and an estrous stage are found at diestrus, as shown in the Venn diagram of significant genes from the comparisons in panel **B**. **D**, Diestrus is likewise the most distinctive transcriptional state within *Cnih3* KO females, illustrated in a Venn of genes significantly DE between any two stages, where the preponderance of stage-pair-specific DEGs correspond to a diestrus comparison. **E**, Table summarizing estrous stage-stage comparisons in WT and KO by number of total DEGs in each genotype and number of shared DEGs across the two genotypes for each stagewise comparison. Full RNA-seq analysis results for comparisons in panels **A–D** are included in Extended Data Table 4-1. *Limma* adjusted RNA-seq log₂(CPM) values after low-expression filtering are in Extended Data Table 4-2 for the entire cohort of WT and KO mice.

and the fact that unitary WT clusters divide up into multiple parts when KO data are also considered, confirmed that the KO estrous cycle patterns of certain subsets of genes were highly divergent from their WT counterparts. In the case of WT cluster 3, our combined-genotypes analysis revealed three subclusters (3.3, 3.5, and 3.7) with attenuated gene upregulation at proestrus in KO mice (Fig. 5B).

To understand functional correlates of these subclusters' combined genes, we performed Enrichr analysis, revealing oligodendrocytes and, interestingly, genes found to be upregulated in estrogen receptor knock-out datasets (Fig. 5C; Extended Data Table 4-1M,N). Likewise, we noticed an attenuation of gene upregulation in KO mice over the diestrus-estrus stages for subclusters 1.2 and 1.4 (Fig. 5D), whose parent cluster had shown enrichment for oligodendrocyte marker genes and potassium channels. Enrichr analysis of these two combined subclusters strikingly revealed that 52 of these 104 genes were in "Mouse Cortex Mature Oligodendrocyte And Progenitor Cell Markers" as defined previously (Doyle et al., 2008); the 104-gene set was also enriched in an additional oligodendrocyte marker list similarly mined from literature (Cahoy et al., 2008), and in various combinations of oligodendrocyte genes identified by single cell RNA-seq (Fig. 5E; Extended Data Table 4-1M,N). Among these genes were *Gpr17*, a factor for oligodendrocyte precursor maturation and myelination (Y. Chen et al., 2009; Lu et al., 2018), and *Srd5a3*, a 5- α reductase that converts testosterone to dihydrotestosterone (DHT; Uemura et al., 2008; Extended Data Fig. 5-2). These findings very strongly suggest that the *Cnih3* KO mouse has specific deficits in oligodendrocyte gene upregulation in response to proestrus.

WT-KO differential expression is unremarkable within sex/estrous stage, against expectations

While above we indirectly compared each contrast in KO to the same contrast in WT, we also directly contrasted the WT and KO mice to better understand effects of the knock-out on dorsal hippocampal gene expression. Contrasting all KO and WT samples, regardless of sex, identified 514 significant DEGs (35 with an absolute log₂FC > 0.5; Fig. 6A), again suggesting overall subtle effects of the *Cnih3* KO on gene expression (Extended Data Table 5-1A). *Enrichr* analysis of these 514 genes revealed highly significant overlap with genes from dozens of brain-relevant transcription factor perturbation experiments, including *Neurod1* knock-down and human cell culture *GATA6* overexpression. This gene set was also highly enriched for protein interactors of estrogen receptor α (*Esr1*). *Cnih3* KO DEGs were also enriched for neuronal markers including those of *Scng*-

expressing interneurons. Intriguingly, and in direct contrast to oligodendrocyte genes with dysregulated cyclic expression patterns in KO, WT versus KO DEGs were instead enriched for genes not expressed in oligodendrocytes relative to other Allen Atlas single-cell RNA-seq cell types (Fig. 6B; Extended Data Table 5-1B).

Subsequently, we performed within-sex/estrous stage comparisons of the two genotypes to better elucidate the effects of *Cnih3* knock-out, given the estrous stage-specific behavioral differences previously seen in these mice (H.E. Frye et al., 2021). Given the extremely large increase in the number of sex- and male-estrous DEGs within KOs, we expected to see comparable numbers of genotype-differential genes within each group. Shockingly, however, only 1–42 FDR-significant DEGs were identified in the genotype comparisons (Extended Data Table 5-1C–G), totaling 63 unique genes (Fig. 6C), with the most differences seen between WT and KO at proestrus. Surprisingly, we observed only one DEG between WT and KO diestrus, despite this stage being responsible for the most DEGs between male and other estrous stages in both WT and KO mice.

Cnih3 KO results in accentuated sex-differential expression compared with WT, especially in diestrus

The findings thus far are surprising when considered in conjunction. Specifically, how is it that KO male versus estrous stage comparisons yielded far more DEGs than did the respective WT comparisons (Extended Data Table 4-1L), while comparing single estrous stages across genotypes yielded a paucity of DEGs (Fig. 6C)? We hypothesized that our findings could be because of subtle KO effects with opposite directions of effect in males and females at certain estrous cycle stages; in other words, we hypothesized that statistically small shifts of KO male expression relative to WT male expression concurrent with statistically small shifts of KO estrous stage expression relative to the same stage in WT could result in more potent DE events between KO males and a given KO stage. Figure 6D confirms this to be the case.

To examine whether this hypothesis was valid at the level of KOs, we first examined the consistency of DE between the two genotypes for each male-stage and stage-stage comparison, as well as the male-all-females comparison. Across these 11 contrasts, 4708 of the 4709 DE events achieving significance (FDR < 0.05) in both genotypes had consistent directionality (Extended Data Table 6-1A), demonstrating the internal reproducibility of the most robust DE patterns, and confirming that *Cnih3* KO did not reverse sex/estrous effects on gene expression. We again used the

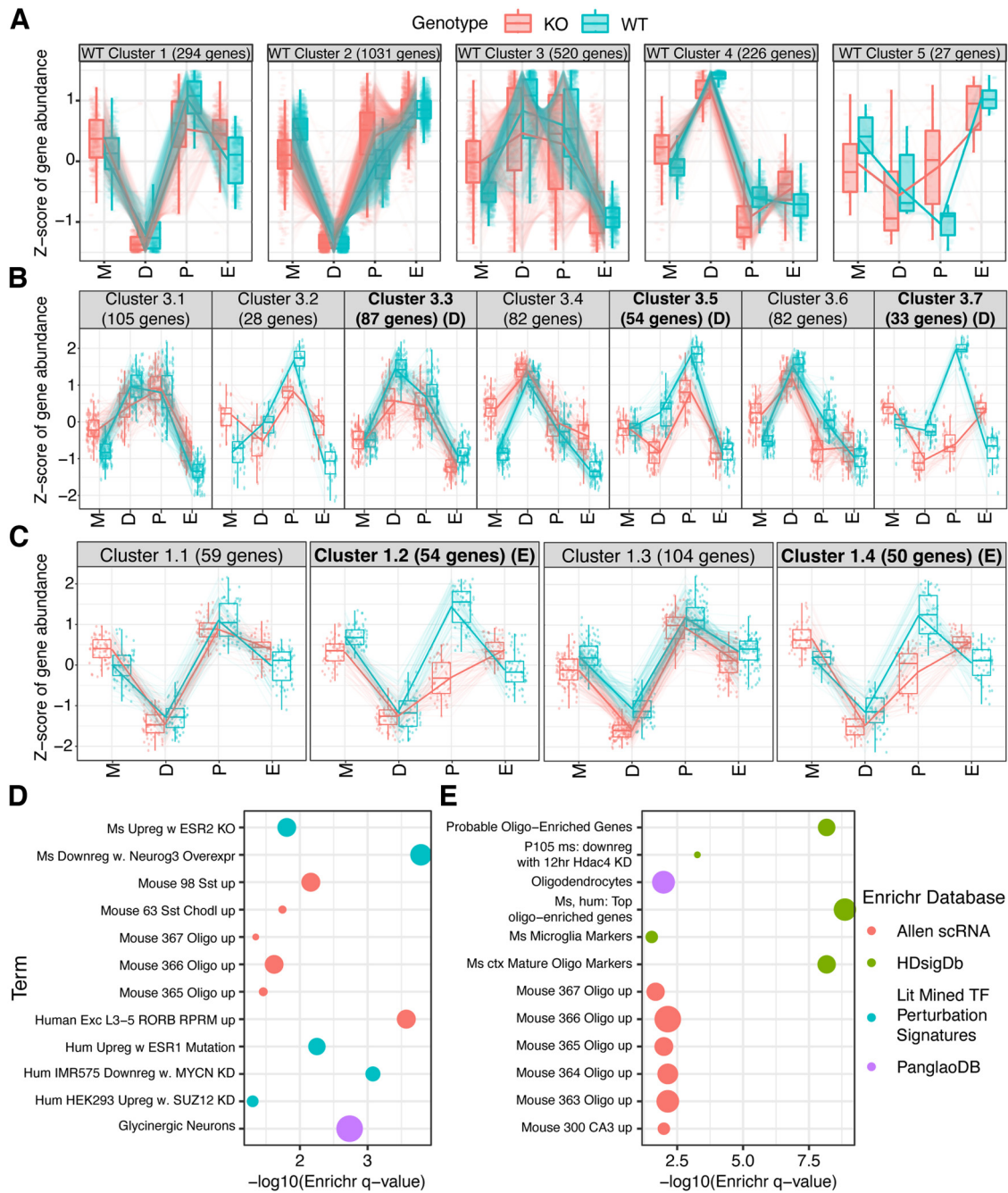


Figure 5. Retained and dysregulated patterns of hippocampal gene expression over the *Cnih3* KO estrous cycle. Note that daily estrous staging in a separate cohort of *Cnih3* KO animals shows unchanged cycle patterns by cytology compared with WT, with staging agreed on by two to three blinded scorers (Extended Data Fig. 5-1). **A**, The same genes from the same five wild-type clusters of cyclic expression shown in Figure 3A are again shown, but now with the KO expression levels of those genes additionally plotted. **B**, Re-clustering of WT cluster 3 using both WT and KO data identified seven subclusters (3.1, 3.2...), corresponding to a specific pattern of regulation in WT and a specific pattern in KO. Three of these clusters (3.3, 3.5, 3.7) show an attenuation of gene upregulation in KO as the cycle progress, especially in the Met → Di and Di → Pro transitions. **C**, Similar re-clustering of WT cluster 1 identified four pattern subgroups, two of which also featured attenuation of upregulation at proestrus compared with WT (1.2, 1.4). **D**, Enrichr analysis of the genes in subclusters 3.3, 3.5, and 3.7 combined highlight that they are DE in estrogen receptor perturbation experiments and enriched in oligodendrocytes and inhibitory neuron classes. **E**, Enrichr analysis of genes in subclusters 1.2 and 1.4 combined were highly enriched for oligodendrocyte genes across several annotation sets, and suggest *Hdac4* as an upstream regulator. Filters for both Enrichr plots are the same as for Figure 3, except with a minimum term-gene set overlap of five rather than eight to account for the smaller gene set sizes of these subclusters. Gene-to-cluster assignments and unabridged Enrichr results for this analysis are in Extended Data Table 5-1. Two example oligodendrocyte genes underlying enrichment results for KO expression pattern subsets showing attenuated upregulation from diestrus to proestrus are shown in Extended Data Figure 5-2.

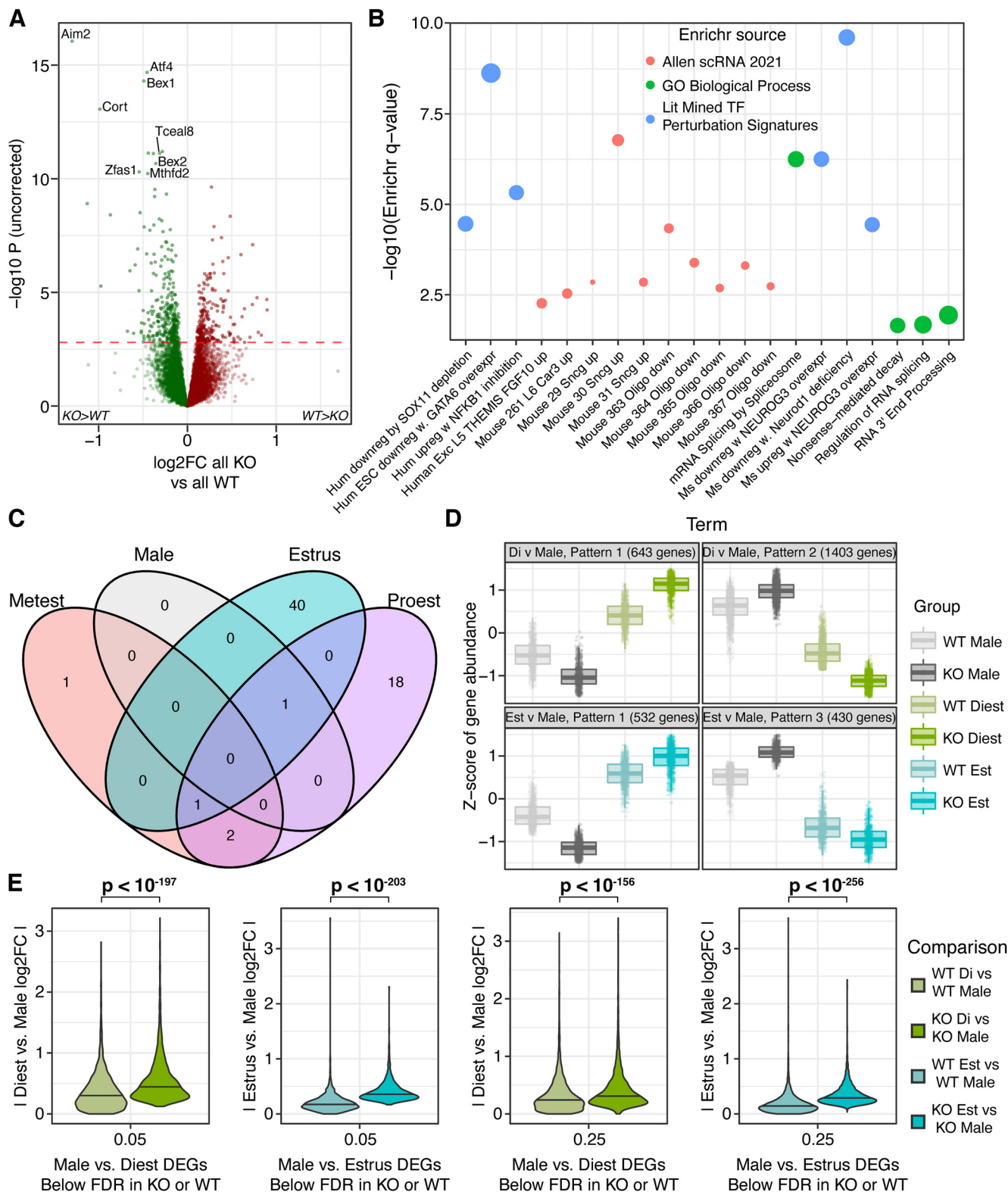


Figure 6. Global features of *Cnih3* KO: Splicing, synuclein, SST, subsurface neurons, and sex difference accentuations. **A**, Comparing all KO to all WT, regardless of sex or estrus stage, identifies hundreds of significant DEGs. **B**, Global DEGs in *Cnih3* KO are enriched for multiple neural subtypes of the mouse brain marked by synuclein γ (*Sncg*), deep layer excitatory neurons, *Sst*-expressing interneurons, and ontology terms related to several forms of RNA processing. Notably, the same oligodendrocyte subtypes identified as *enriched* for genes dysregulated in the KO estrous cycle are depleted (i.e., lowly-expressed) in the global DEGs of the KO mouse. All terms plotted were nominally significant for enrichment and met filters for a minimum log OR of two and a minimum of eight DEGs overlapping with the annotation term set. **C**, A surprisingly small number of DEGs are identified by comparing

continued

single estrous stages or males between KO and WT. (Stages not shown have 0 significant DEGs.) **D**, Analysis of genes DE between KO males and a KO estrous stage at $FDR < 0.01$ showed several sizable groups of genes where *Cnih3* KO accentuated a normal sex difference seen in WT—that is, a greater magnitude of effect in KOs while with the same effect direction as found in WT. The illustrated gene sets show a larger difference between KO males and KO females (in opaque colors) compared with the same male-stage pairs in WT (translucent colors) at the illustrated stages. **E**, The range of absolute \log_2 fold-changes for the union of DEGs from WT and KO male-diestrus comparisons or from WT and KO male-estrus comparisons at multiple FDR cutoffs. At all FDR thresholds examined, the absolute magnitude of DE is significantly (Wilcoxon test) greater in the KO comparison, indicating virtually global potentiation of estrous stage-specific sex-differential expression in KOs. The RNA-seq analysis results of global KO-WT comparison, gene-to-cluster assignments, and unabridged Enrichr results for male-versus-estrous stage effect patterns in WT versus KO are in Extended Data Table 6-1.

degPattern algorithm to visually compare WT expression of KO male-estrous DEGs. Consistent with our hypothesis, we see that KO DEGs generally show exaggerated effect magnitudes relative to their WT peers. The overall conclusion is that KOs have accentuated sex differences across large portions of the dorsal hippocampal transcriptome (Fig. 6D; shown are the two KO estrous stage-male comparisons with the most DEGs; Extended Data Table 6-1B,C). Enrichr analyses of genes following each pattern for these two male-stage comparisons (such as male > diestrus in WT with male upregulation and female downregulation in KO) are provided in Extended Data Table 6-1D, and recurring terms across genes with different patterns are tabulated in Extended Data Table 6-1E.

To confirm accentuated sex differences in the KOs, we also examined all genes differentially expressed in either genotype between males and diestrus or between males and estrus, and plotted their absolute \log_2 fold change values for both WT and KO mice (Fig. 6E). At any FDR thresholds tested, a nonparametric Wilcoxon test identified an extremely significant increase in the magnitude of the absolute sex differences in the KO compared with those seen in WT. This confirms the observation of a general net increase in sex-differential expression between *Cnih3* KO males and KO females during diestrus and estrus.

Discussion

We had a variety of motivations for specifically conducting a study on estrous-regulated gene expression in the dorsal hippocampus of both WT and *Cnih3* KO mice. Prior work has demonstrated the influence of estrous stage on both hippocampal physiology and spatial learning (C.A. Frye, 1995; Warren and Juraska, 1997), highlighting the important influences of reproductive physiology on behavior and hippocampal activity. The dorsal hippocampus is an important site of integration of sex hormone and stress signaling (Bao et al., 2006; Frick et al., 2015; Padilla-Coreano et al., 2016); stress plays key roles in drug reinstatement (McKee et al., 2015) and likely psychotic disorders (Walker et al., 2013), and interestingly, is also influenced from upstream by sex through the HPA axis (Lund et al., 2004). The dorsal hippocampus is therefore of special interest in *Cnih3* mutant mice because of the association of *CNIH3* to addiction phenotypes and schizophrenia in humans (Drummond et al., 2012; Nelson et al., 2016) and reported mouse knock-out interactions with sex and estrous affecting hippocampal learning phenotypes

and glutamatergic signaling pathways (H.E. Frye et al., 2021). We thus conducted a well-powered study to understand the transcriptional effects of estrous on dorsal hippocampal gene expression in both wild-type and *Cnih3* KO animals. Our results provide valuable insights to help future studies to dissect the interactions and mechanisms for sex/hormone-dependent *Cnih3* roles in behavioral learning and substance use disorder risk.

We found that on average, the brain is well buffered against sex differences in expression, with the WT gene expression showing few differences between males and females (mostly sex chromosomal). Surprisingly, we only detect DE for a handful of genes known to escape X-inactivation in mouse brain (Berletch et al., 2015) or previously reported to be sex-differentially expressed in mouse hippocampus (Vied et al., 2016; Bundy et al., 2017). This discrepancy may be because of the low likelihood of the prior estrous-agnostic sex DE studies having a balanced representation of estrous stages because of the brevity (hours) of certain stages, like estrus, and extended duration of other stages, like diestrus. Supporting this notion, a recent examination of four prior mouse hippocampal sex DE studies (Ocañas et al., 2022) identified only eight consensus sex chromosomal DEGs, all of which are in the top 11 DEGs from our WT male-female comparison as ranked by FDR.

Meanwhile, at specific stages of the estrous cycle, females differed more substantially from males. Likewise, estrous stages also showed differential expression between one another; in comparing single stages against one another or to males, diestrus was consistently the most transcriptionally distinct state from males and from other stages of the estrous cycle. Consistent with our findings of a distinctive diestrus hippocampal transcriptome, and perhaps explaining discrepancies with prior sex DE studies, it has recently been shown that chrX chromatin structure in mouse ventral hippocampus is similar between proestrus females and males, but substantially different from both at diestrus (Rocks et al., 2022).

We examined data from wild-type females and identified various changes across estrous cycle phases that may have interesting biological relevance to estrous cycle specific changes in dorsal hippocampal physiology and behavior. For genes in cluster 1, with trough expression in diestrus and peak expression in proestrus—a period over which estradiol goes from lowest to highest, and progesterone starts high and begins to decrease, we observed enrichment in oligodendrocyte markers. Myelin, which is made by oligodendrocytes and increases efficiency of

synaptic transmission, has been shown to increase after increased neuronal activity in the motor cortex (Gibson et al., 2014), and this was necessary for the motor function enhancement seen in their system. It is interesting to note that long-term potentiation (LTP), which is characterized by increased neuronal transmission, is enhanced during proestrus (Warren et al., 1995) with some reporting improved object-based spatial learning during this phase (C. A. Frye, 1995). Thus, it is possible that changes in myelination might help support this increased LTP and learning. For genes in cluster 2, with peak expression in estrus/metestrus and trough expression in diestrus, a period over which estradiol declines and fluctuates from its initial peak at estrus, while progesterone starts low and increases, we observed enrichment in genes involved in calcium and glutamate receptor signaling. Previous research has shown that estradiol improves recognition and spatial learning, and increases hippocampal spine density in CA1 (Woolley and McEwen, 1993), which requires calcium and glutamate receptor signaling. Thus, it will be interesting to investigate whether the receptors upregulated here mediate improved spatial learning seen at this phase. Regardless, our results suggest that behaviorists may wish to measure estrus state and include it as a covariate in their analyses, especially when assessing behaviors related to the dorsal hippocampus.

We then examined data from *Cnih3* knock-outs in the same manner, identifying a much more marked extent of sex-differential expression when clumping all estrous stages together, and likewise between males and single stages. Using our WT estrous cycle gene expression patterns, and given the estrous-stage-specific behavioral changes previously observed in *Cnih3* KO mice (H.E. Frye et al., 2021), we examined whether KO expression patterns deviated from WT over the estrous cycle. We indeed identified specific subsets of genes with blunted upregulation in KO over estrogenic stages of the cycle, especially proestrus. These dysregulated gene subsets overlapped with markers of oligodendrocytes, glycinergic neurons, and somatostatin (SST) interneurons, indicating these cell types might be most impacted by *Cnih3* mutation. Pathway analysis indicated these genes were disproportionately downstream of a handful of regulators including *Hdac4*, *Klf4*, *Neurog3*, and the estrogen receptor *Esr1*, suggesting the consequences of *Cnih3* mutation might work through these molecular pathways. Consistent with hippocampal biology and its role in memory, *Hdac4* and *Neurog3* are involved in regulating dendritic morphology (Simon-Arces et al., 2010; Litke et al., 2018), while *Klf4* plays a role in regulating neural stem cell self-renewal (Qin et al., 2011). However, more work would need to be done to test specific roles of these genes downstream of *Cnih3* KO.

Cnih3 was of interest because human genetic association studies suggest polymorphism in this region may be protective against opioid dependence (Nelson et al., 2016), a disease that involves hijacking of normal reward mechanisms including learning and memory (i.e., dorsal hippocampal) processes. CNIH3 has been shown to bind AMPARs and alter synaptic AMPAR trafficking, gating, and signaling (Schwenk et al., 2009; Coombs et al., 2012;

Shanks et al., 2014; Brown et al., 2018). An initial study of hippocampal slice physiology phenotypes suggested little function for *Cnih3*, except in the context of co-deletion of *Cnih2*: when both proteins were deleted, physiological studies in the acute slices revealed a phenocopy of several aspects of GluA1 KO (a subunit of AMPARs), including altered mEPSC amplitude and kinetics, and deficits in long-term potentiation (Herring et al., 2013). However, behavioral effects were not assessed; notably, these slices were all generated from prepubescent animals, as is standard in the field, precluding characterization of adult *Cnih3* function and hormonal influences on it. Finally, a recent investigation of hippocampal learning and memory function via Barnes maze in *Cnih3* KO mice revealed no main effects of genotype initially, but a surprising amount of variance in females. Subsequent exploration of this led to the discovery of estrous-stage specific effects of both *Cnih3* KO and hippocampus-specific *Cnih3* overexpression (H.E. Frye et al., 2021). Furthermore, synaptic physiology (in adult slices) as well as biochemical and immunofluorescent analyses of synapses revealed stage specific alterations in dorsal hippocampal properties across multiple levels. All of these results led us to the hypothesis that *Cnih3* in some way buffers against hormone-dependent sex differences, with the loss of the protein unmasking deficits in KO females.

We therefore directly examined expression differences in WT versus KO altogether and between males or estrous stages. The 514 genes we identified as differentially expressed between genotypes highlighted some shared enrichments with estrous-(dys)regulated gene sets at the level of cell types (SST interneurons, *Scng*-expressing neurons) and transcriptional regulators (*Neurog3*); however, most functional enrichments were distinct, spanning several forms of RNA processing and transport, and candidate upstream regulators. These included *Neurod1*, *Hsp90*, and, interestingly, X-binding protein 1 (*Xbp1*). When we compared single estrous stages or males across genotypes, however, we identified very little differential expression. The combined observation of broader differential expression between male and estrous stages within KOs compared with within WTs, despite the absence of genotype differences, suggested to us that subtle changes were being induced by *Cnih3* KO to accentuate sex-differential expression. Indeed, we observed that the magnitude of sex-differential expression at diestrus or estrus was consistently greater in the KO (Fig. 6E), confirming our hypothesis that *Cnih3* buffers against excess gene-regulatory responses to cycling sex hormones.

Our study did have several limitations. Some previous studies examining estrous stage and hippocampal biology have performed extensive estrous staging across multiple cycles (Woolley and McEwen, 1992; Jaric et al., 2019), whereas here, we only performed cytologic staging on two consecutive days (the day before tissue collection and at tissue collection), which could potentially lead to inclusion of brains from mice with irregular cycling. Additionally, the cytologic diestrus phase consists of endocrinologically distinct early (low estrogen) and late (rising estrogen) phases. Future studies using the *Cnih3* global KO mouse line would benefit from serum hormonal profiling of estrous cycling to

examine potential for gonadal-endocrine mechanism of the KO effect. Nonetheless, observations from 11 to 14 d of daily estrous staging in independent WT and KO mice ($n=27$ per genotype) suggest that, cytologically, cycling is intact in KO animals (Extended Data Fig. 5-1).

Our sample clustering (Fig. 2E) suggests that a portion of our WT diestrus mice may have been split between two transcriptional states, which most likely represented these endocrine subphases. We note, however, that the two subclusters of WT diestrus samples are similarly sized, such that our overall data for WT at diestrus should represent the composite cytologic stage. Additionally, three-dimensional principal component analysis plotting of genes with highly variable expression across groups (≥ 1 SD) showed that this pattern was not unique to diestrus when either including (Extended Data Fig. 2-2) or excluding (Extended Data Fig. 2-3) sex chromosomes. Finally, we were deliberately permissive in our thresholds for calling DEGs (only requiring an $FDR < 0.05$ without an additional fold-change cutoff). While this procedure will result in detection of some smaller magnitude changes at the level of single genes, it aids our gestalt analysis by casting a broader net for genes subject to any degree of significant fluctuation across the estrous cycle.

Altogether, we deeply characterize dorsal hippocampal gene expression patterns across the estrous cycle in WT mice, characterize the *Cnih3* KO dorsal hippocampal transcriptome, and identify a surprising potentiation of sex-differential gene expression in this knock-out line. The data and supplements from these analyses provide extensive gene annotations for WT regulatory patterns, their dysregulation in *Cnih3* KO, and a well-powered dataset illustrating the role of estrous stage in defining sex-differential gene expression. Thus, these analyses and data provide a resource for the study of sex- and estrous-differential gene expression in the mouse dorsal hippocampus.

References

- Arnold AP (2009) The organizational-activational hypothesis as the foundation for a unified theory of sexual differentiation of all mammalian tissues. *Horm Behav* 55:570–578.
- Bao AM, Fischer DF, Wu YH, Hol EM, Balesar R, Unmehopa UA, Zhou JN, Swaab DF (2006) A direct androgenic involvement in the expression of human corticotropin-releasing hormone. *Mol Psychiatry* 11:567–576.
- Barth C, Steele CJ, Mueller K, Rekkas VP, Arélin K, Pampel A, Burmann I, Kratzsch J, Villringer A, Sacher J (2016) In-vivo dynamics of the human hippocampus across the menstrual cycle. *Sci Rep* 6:32833.
- Berletch JB, Ma W, Yang F, Shendure J, Noble WS, Disteche CM, Deng X (2015) Escape from X inactivation varies in mouse tissues. *PLoS Genet* 11:e1005079.
- Brown PMGE, McGuire H, Bowie D (2018) Stargazin and cornichon-3 relieve polyamine block of AMPA receptors by enhancing blocker permeation. *J Gen Physiol* 150:67–82.
- Bundy JL, Vied C, Nowakowski RS (2017) Sex differences in the molecular signature of the developing mouse hippocampus. *BMC Genomics* 18:237.
- Cahoy JD, Emery B, Kaushal A, Foo LC, Zamanian JL, Christopherson KS, Xing Y, Lubischer JL, Krieg PA, Krupenko SA, Thompson WJ, Barres BA (2008) A transcriptome database for astrocytes, neurons, and oligodendrocytes: a new resource for understanding brain development and function. *J Neurosci* 28:264–278.
- Chen EY, Tan CM, Kou Y, Duan Q, Wang Z, Meirelles GV, Clark NR, Ma'ayan A (2013) Enrichr: interactive and collaborative HTML5 gene list enrichment analysis tool. *BMC Bioinformatics* 14:128.
- Chen Y, Wu H, Wang S, Koito H, Li J, Ye F, Hoang J, Escobar SS, Gow A, Arnett HA, Trapp BD, Karandikar NJ, Hsieh J, Lu QR (2009) The oligodendrocyte-specific G-protein coupled receptor GPR17 is a cell-intrinsic timer of myelination. *Nat Neurosci* 12:1398–1406.
- Coombs ID, Soto D, Zonouzi M, Renzi M, Shelley C, Farrant M, Cull-Candy SG (2012) Cornichons modify channel properties of recombinant and glial AMPA receptors. *J Neurosci* 32:9796–9804.
- Del Río JP, Alliende MI, Molina N, Serrano FG, Molina S, Vigil P (2018) Steroid hormones and their action in women's brains: the importance of hormonal balance. *Front Public Health* 6:141.
- DiCarlo LM, Vied C, Nowakowski RS (2017) The stability of the transcriptome during the estrous cycle in four regions of the mouse brain. *J Comp Neurol* 525:3360–3387.
- Dobin A, Davis CA, Schlesinger F, Drenkow J, Zaleski C, Jha S, Batut P, Chaisson M, Gingeras TR (2013) STAR: ultrafast universal RNA-seq aligner. *Bioinformatics* 29:15–21.
- Doyle JP, Dougherty JD, Heiman M, Schmidt EF, Stevens TR, Ma G, Bupp S, Shrestha P, Shah RD, Doughty ML, Gong S, Greengard P, Heintz N (2008) Application of a translational profiling approach for the comparative analysis of CNS cell types. *Cell* 135:749–762.
- Drummond JB, Simmons M, Haroutunian V, Meador-Woodruff JH (2012) Upregulation of cornichon transcripts in the dorsolateral prefrontal cortex in schizophrenia. *Neuroreport* 23:1031–1034.
- Duclot F, Kabbaj M (2015) The estrous cycle surpasses sex differences in regulating the transcriptome in the rat medial prefrontal cortex and reveals an underlying role of early growth response 1. *Genome Biol* 16:256.
- Fakira AK, Massaly N, Cohensedgh O, Berman A, Morón JA (2016) Morphine-associated contextual cues induce structural plasticity in hippocampal CA1 pyramidal neurons. *Neuropsychopharmacology* 41:2668–2678.
- Frick KM, Kim J (2018) Mechanisms underlying the rapid effects of estradiol and progesterone on hippocampal memory consolidation in female rodents. *Horm Behav* 104:100–110.
- Frick KM, Kim J, Tuscher JJ, Fortress AM (2015) Sex steroid hormones matter for learning and memory: estrogenic regulation of hippocampal function in male and female rodents. *Learn Mem* 22:472–493.
- Frye CA (1995) Estrus-associated decrements in a water maze task are limited to acquisition. *Physiol Behav* 57:5–14.
- Frye HE, Izumi Y, Harris AN, Williams SB, Trousdale CR, Sun MY, Sauerbeck AD, Kummer TT, Mennerick S, Zorumski CF, Nelson EC, Dougherty JD, Morón JA (2021) Sex differences in the role of CNH3 on spatial memory and synaptic plasticity. *Biol Psychiatry* 90:766–780.
- Gibson EM, Purger D, Mount CW, Goldstein AK, Lin GL, Wood LS, Inema I, Miller SE, Bieri G, Zuchero JB, Barres BA, Woo PJ, Vogel H, Monje M (2014) Neuronal activity promotes oligodendrogenesis and adaptive myelination in the mammalian brain. *Science* 344:1252304.
- Henderson YO, Victoria NC, Inoue K, Murphy AZ, Parent MB (2015) Early life inflammatory pain induces long-lasting deficits in hippocampal-dependent spatial memory in male and female rats. *Neurobiol Learn Mem* 118:30–41.
- Herring BE, Shi Y, Suh YH, Zheng C-Y, Blankenship SM, Roche KW, Nicoll RA (2013) Cornichon proteins determine the subunit composition of synaptic AMPA receptors. *Neuron* 77:1083–1096.
- Iqbal J, Tan ZN, Li MX, Chen HB, Ma B, Zhou X, Ma XM (2020) Estradiol alters hippocampal gene expression during the estrous cycle. *Endocr Res* 45:84–101.
- Jaric I, Rocks D, Cham H, Herchek A, Kundakovic M (2019) Sex and estrous cycle effects on anxiety- and depression-related phenotypes in a two-hit developmental stress model. *Front Mol Neurosci* 12:74.
- Johnson MA, Contoreggi NH, Kogan JF, Bryson M, Rubin BR, Gray JD, Kreek MJ, McEwen BS, Milner TA (2021) Chronic stress

- differentially alters mRNA expression of opioid peptides and receptors in the dorsal hippocampus of female and male rats. *J Comp Neurol* 529:2636–2657.
- Kessels HW, Malinow R (2009) Synaptic AMPA receptor plasticity and behavior. *Neuron* 61:340–350.
- Kohtz AS, Aston-Jones G (2016) Cocaine seeking during initial abstinence is driven by noradrenergic and serotonergic signaling in hippocampus in a sex-dependent manner. *Neuropsychopharmacology* 42:408–418.
- Kuhn C (2015) Emergence of sex differences in the development of substance use and abuse during adolescence. *Pharmacol Ther* 153:55–78.
- Lee HK, Takamiya K, Han JS, Man H, Kim CH, Rumbaugh G, Yu S, Ding L, He C, Petralia RS, Wenthold RJ, Gallagher M, Huganir RL (2003) Phosphorylation of the AMPA receptor GluR1 subunit is required for synaptic plasticity and retention of spatial memory. *Cell* 112:631–643.
- Li Y, Ge X, Peng F, Li W, Li JJ (2022) Exaggerated false positives by popular differential expression methods when analyzing human population samples. *Genome Biol* 23:79.
- Litke C, Bading H, Mauceri D (2018) Histone deacetylase 4 shapes neuronal morphology via a mechanism involving regulation of expression of vascular endothelial growth factor D. *J Biol Chem* 293:8196–8207.
- Liu R, Holik AZ, Su S, Jansz N, Chen K, Leong HS, Blewitt ME, Asselin-Labat M-L, Smyth GK, Ritchie ME (2015) Why weight? Modelling sample and observational level variability improves power in RNA-seq analyses. *Nucleic Acids Res* 43:e97.
- Liu C, Dong L, Zhou H, Li Q, Huang G, Bai S, Liao L (2018) G-protein-coupled receptor Gpr17 regulates oligodendrocyte differentiation in response to lysolecithin-induced demyelination. *Sci Rep* 8:4502.
- Lund TD, Munson DJ, Halcy ME, Handa RJ (2004) Androgen inhibits, while oestrogen enhances, restraint-induced activation of neuro-peptide neurones in the paraventricular nucleus of the hypothalamus. *J Neuroendocrinol* 16:272–278.
- McKee SA, Potenza MN, Kober H, Sofuoglu M, Arnsten AFT, Picciotto MR, Weinberger AH, Ashare R, Sinha R (2015) A translational investigation targeting stress-reactivity and prefrontal cognitive control with guanfacine for smoking cessation. *J Psychopharmacol* 29:300–311.
- Nelson EC, et al. (2016) Evidence of CNH3 involvement in opioid dependence. *Mol Psychiatry* 21:608–614.
- Ocañas SR, Ansere VA, Tooley KB, Hadad N, Chucair-Elliott AJ, Stanford DR, Rice S, Wronowski B, Pham KD, Hoffman JM, Austad SN, Stout MB, Freeman WM (2022) Differential regulation of mouse hippocampal gene expression sex differences by chromosomal content and gonadal sex. *Mol Neurobiol* 59:4669–4702.
- Padilla-Coreano N, Bolkan SS, Pierce GM, Blackman DR, Hardin WD, Garcia-Garcia AL, Spellman TJ, Gordon JA (2016) Direct ventral hippocampal-prefrontal input is required for anxiety-related neural activity and behavior. *Neuron* 89:857–866.
- Pantano L, Hutchinson J, Barrera V, Piper M, Khetani R, Daily K, Perumal TM, Kirchner R, Steinbaugh M (2022) DEGreport: Report of DEG analysis. R package version 1.34.0. Available at <http://lpantano.github.io/DEGreport/>.
- Portugal GS, Al-Hasani R, Fakira AK, Gonzalez -Romero JL, Melyan Z, McCall JG, Bruchas MR, Morón JA (2014) Hippocampal long-term potentiation is disrupted during expression and extinction but is restored after reinstatement of morphine place preference. *J Neurosci* 34:527–538.
- Qin S, Liu M, Niu W, Zhang C-L (2011) Dysregulation of Kruppel-like factor 4 during brain development leads to hydrocephalus in mice. *Proc Natl Acad Sci U S A* 108:21117–21121.
- Ritchie ME, Phipson B, Wu D, Hu Y, Law CW, Shi W, Smyth GK (2015) limma powers differential expression analyses for RNA-seq and microarray studies. *Nucleic Acids Res* 43:e47.
- Robinson MD, McCarthy DJ, Smyth GK (2010) edgeR: a bioconductor package for differential expression analysis of digital gene expression data. *Bioinformatics* 26:139–140.
- Rocks D, Shukla M, Ouldibbat L, Finnemann SC, Kalluchi A, Rowley MJ, Kundakovic M (2022) Sex-specific multi-level 3D genome dynamics in the mouse brain. *Nat Commun* 13:3438.
- Schwenk J, Harmel N, Zolles G, Bildl W, Kulik A, Heimrich B, Chisaka O, Jonas P, Schulte U, Fakler B, Klöcker N (2009) Functional proteomics identify cornichon proteins as auxiliary subunits of AMPA receptors. *Science* 323:1313–1319.
- Shanks NF, Cais O, Maruo T, Savas JN, Zaika EI, Azumaya CM, Yates JR, Greger I, Nakagawa T (2014) Molecular dissection of the interaction between the AMPA receptor and cornichon homolog-3. *J Neurosci* 34:12104–12120.
- Simon-Areces J, Membrive G, Garcia-Fernandez C, Garcia-Segura LM, Arevalo M-A (2010) Neurogenin 3 cellular and subcellular localization in the developing and adult hippocampus. *J Comp Neurol* 518:1814–1824.
- Uemura M, Tamura K, Chung S, Honma S, Okuyama A, Nakamura Y, Nakagawa H (2008) Novel 5 α -steroid reductase (SRD5A3, type-3) is overexpressed in hormone-refractory prostate cancer. *Cancer Science* 99:81–86.
- Vied C, Ray S, Badger C-D, Bundy JL, Arbeitman MN, Nowakowski RS (2016) Transcriptomic analysis of the hippocampus from six inbred strains of mice suggests a basis for sex-specific susceptibility and severity of neurological disorders. *J Comp Neurol* 524:2696–2710.
- Walker EF, Trotman H, Pearce BD, Addington J, Cadenhead KS, Cornblatt BA, Heinssen R, Mathalon DH, Perkins DO, Seidman LJ, Tsuang MT, Cannon TD, McGlashan TH, Woods SW (2013) Cortisol levels and risk for psychosis: initial findings from the North American prodrome longitudinal study. *Biol Psychiatry* 74:410–417.
- Warren SG, Juraska JM (1997) Spatial and nonspatial learning across the rat estrous cycle. *Behav Neurosci* 111:259–266.
- Warren SG, Humphreys AG, Juraska JM, Greenough WT (1995) LTP varies across the estrous cycle: enhanced synaptic plasticity in proestrus rats. *Brain Res* 703:26–30.
- Woolley CS, McEwen BS (1992) Estradiol mediates fluctuation in hippocampal synapse density during the estrous cycle in the adult rat. *J Neurosci* 12:2549–2554.
- Woolley CS, McEwen BS (1993) Roles of estradiol and progesterone in regulation of hippocampal dendritic spine density during the estrous cycle in the rat. *J Comp Neurol* 336:293–306.
- Xia Y, Portugal GS, Fakira AK, Melyan Z, Neve R, Lee HT, Russo SJ, Liu J, Morón JA (2011) Hippocampal GluA1-containing AMPA receptors mediate context-dependent sensitization to morphine. *J Neurosci* 31:16279–16291.
- Zhang Y, Parmigiani G, Johnson WE (2020) ComBat-seq: batch effect adjustment for RNA-seq count data. *NAR Genom Bioinform* 2:lqaa078.